Neutrophil-Vasculature Interactions Promote Pro-Recurrent Niche Formation Post-Radiotherapy

Shannon Martello[1], Gladys Martinez-Franco[2], Kirsten Stubenrauch[1], Bridget Stevenson[3], Holden Korbey[4], Kevin Corn[1], Tian Zhu[1], and Marjan Rafat[1,3,5]

[1]Department of Chemical and Biomolecular Engineering, Vanderbilt University
[2]Department of Chemical and Materials Engineering, California State Polytechnic University, Pomona
[3]Department of Biomedical Engineering, Vanderbilt University
[4]Department of Biological Sciences, Vanderbilt University
[5]Department of Radiation Oncology, Vanderbilt University Medical Center

Contact: shannon.e.martello@vanderbilt.edu

Motivation & Background

- Despite aggressive treatment with chemotherapy, surgery, and radiotherapy (RT), triple negative breast cancer (TNBC) has a high rate of locoregional recurrence, especially among lymphopenic patients [1, 2].
- RT-induced damage to the mammary adipose tissue recruits macrophages and circulating tumor cells (CTCs) in lymphopenic mice (**Fig. 1**).
- A high neutrophil-to-lymphocyte ratio (NLR) after adjuvant RT is a prognostic marker for local TNBC recurrence (**Fig. 2**), suggesting that neutrophils facilitate a microenvironment favorable for CTC reseeding[3].
- The vasculature is a key component of cell and nutrient transport through tissue, yet the role of vascular changes and neutrophil-vasculature interactions in TNBC recurrence are unclear.
- We are currently studying how neutrophils contribute to TNBC recurrence through interactions with radiation-damaged vasculature.

References:

1. AJ Lowery *et al.* (2011) *Breast Cancer Res Treat*
2. M Rafat *et al.* (2018) *Cancer Res*
3. A Sherry *et al.* (2020) *Int J Rad Onc Bio Phys*

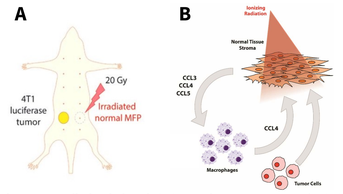

Figure 1: Radiation-induced CTC recruitment. A. To study CTC recruitment to irradiated normal tissue, luciferase-labeled 4T1 ($4T1^{luc}$) cells were injected into the #4 mammary fat pad (MFP) of BALB/c mice. **B.** Irradiated normal tissue secretes factors that recruit macrophages and CTCs [2].

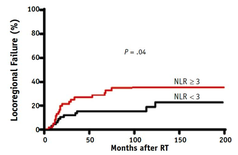

Figure 2: High NLR is associated with increased risk of locoregional TNBC failure post-RT. Patients with NLR ≥ 3 after RT had higher incidence of locoregional recurrence compared to patients with NLR < 3 [3].

Methods and Results

Recurrence Model

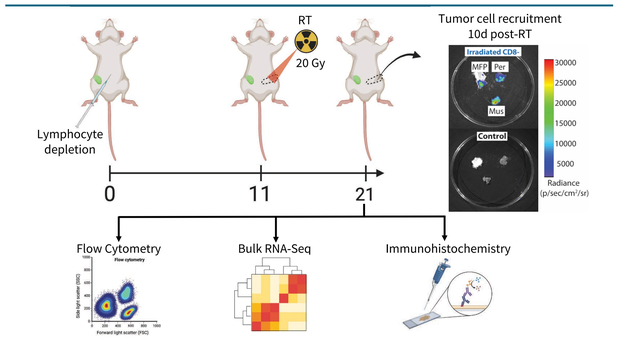

Figure 3: *In vivo* model of CTC recruitment. $4T1^{luc}$ cells were injected into the left #4 MFP of female BALB/c mice. At the time of tumor inoculation, mice also received an i.p. injection of anti-CD8 or anti-IgG control antibodies, which were injected every 5 days thereafter. When tumors reached 100 mm^3, the contralateral #4 MFP was irradiated. Mice were sacrificed at 10d post-RT. Contralateral MFPs were resected and processed for flow cytometry, bulk RNA-sequencing, or immunohistochemistry (IHC). Tumor cell recruitment is visible via bioluminescent imaging at 10d[2].

Activation of neutrophils in mammary adipose tissue corresponds with tumor cell infiltration 10 days post-radiation

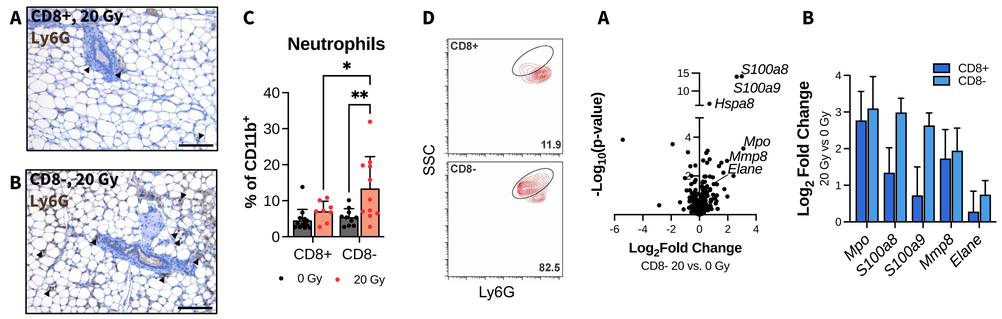

Figure 4: Neutrophils exhibit signs of activation in MFPs 10d post-RT. Representative images of Ly6G⁺ cells in MFPs 10d post-RT in **(A)** immunocompetent (CD8+) and **(B)** immunocompromised (CD8-) mice. Scale bars are 100 µm. **C.** Quantification of $CD45^+CD11b^+Ly6C^-Ly6G^+SSC^{hi}$ neutrophils in MFPs at 10d post-RT analyzed via flow cytometry. n=8-12 mice. Error bars show SD. **D.** Representative contour plots of neutrophils in 20 Gy MFPs of CD8+ and CD8- mice at 10d post-RT. Oval indicates gating for SSC^{hi} neutrophils.

Figure 5: Significant upregulation of neutrophil degranulation-related genes in CD8- mice 10d post-RT. A. Volcano plot of neutrophil degranulation pathway gene expression from bulk RNA-seq analysis of irradiated and unirradiated CD8- MFPs. **B.** Gene expression of select neutrophil granule proteins in CD8- and CD8+ mice in 20 vs. 0 Gy MFPs. n=5 mice per condition. Error bars show SD.

Vascular remodeling in CD8- mice 10 days post-radiation

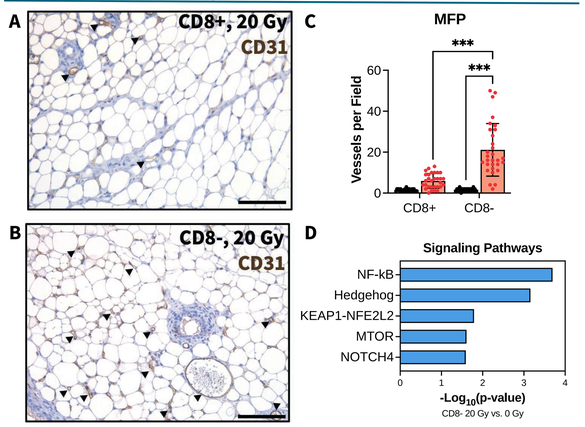

Figure 6: Vascular changes in MFPs at 10d post-RT. Representative images of CD31 IHC staining in MFPs of **(A)** CD8+ and **(B)** CD8- mice 10d post-RT. Scale bars are 100 µm. Arrows indicate $CD31^+$ vessels. **C.** Quantification of $CD31^+$ vessel counts in MFPs 10d post-RT. n=3 mice per condition. Each point is one field of view with 10 fields of view per mouse. Error bars are SD with *p<0.05 and **p<0.01 by ANOVA. **D.** Significantly enriched pathways related to tissue remodeling in irradiated CD8- mice determined by Reactome analysis of MFP RNA-seq data. n=5 mice per condition.

Tumors in pre-irradiated tissue exhibit increased vessel formation

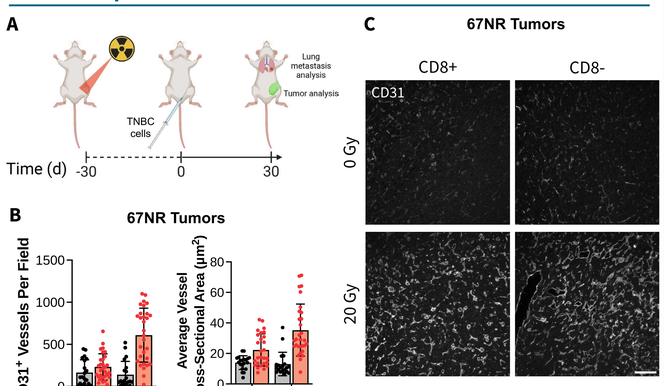

Figure 7: Tumors in pre-irradiated CD8- tumor beds exhibit similar characteristics to normal MFP changes post-RT. A. Experimental timeline: MFPs of CD8+ and CD8- mice were irradiated to 20 Gy. 4T1 (not shown) or 67NR TNBC cells were inoculated into irradiated tissue 30d post-RT. Organs were collected 30d post-inoculation for primary and distant tumor analyses. **B.** Quantification of $CD31^+$ vessel counts and area from IHC-IF staining of 67NR tumors. Each point is one field of view with 10 fields of view per mouse. Error bars show SD. n=2-3 mice per condition. **C.** Representative images of CD31 IHC-IF staining of 67NR tumors. Scale bar=100 µm.

Neutrophil-endothelial cell interactions *in vitro*

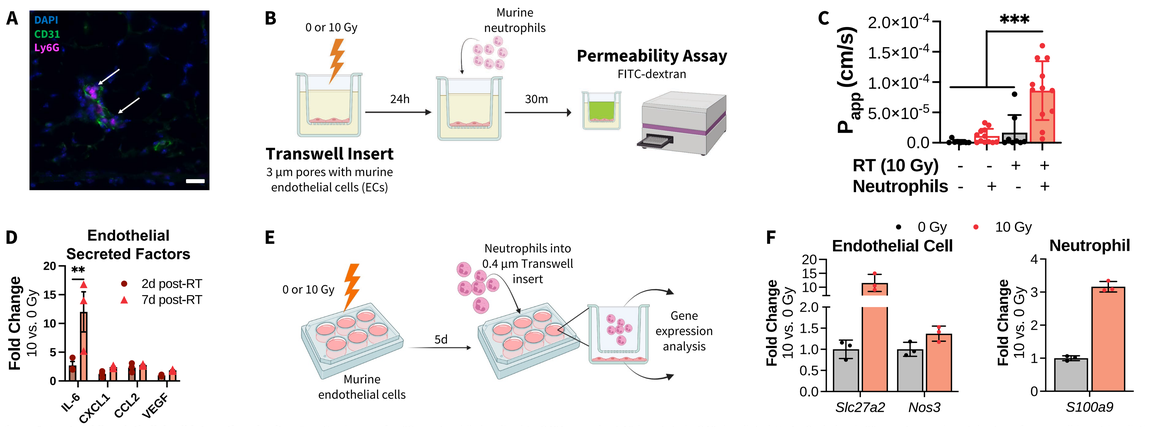

Figure 8: Neutrophil-endothelial cell interactions *in vitro*. A. IHC-IF image of Ly6G⁺ neutrophils localized to $CD31^+$ vessels at 10d post-RT in CD8- irradiated MFPs. Scale bar is 20 µm. **B.** Experimental setup of Transwell insert irradiation, neutrophil addition, and quantification of endothelial monolayer permeability. **C.** Quantification of endothelial monolayer permeability post-RT and –neutrophil migration. n= 7-9 biological replicates. ***p<0.001 by ANOVA. **D.** Significantly upregulated cytokines secreted by ECs 2 and 7d post-RT. **E.** Experimental setup of indirect neutrophil-EC 24h co-culture at 5d post-RT of ECs. **F.** RT-qPCR analysis of angiogenesis- and inflammation-related genes in ECs and neutrophils after 24h of indirect co-culture. n=1 biological replicate. Error bars show SD.

In vitro Model Development

Device fabrication

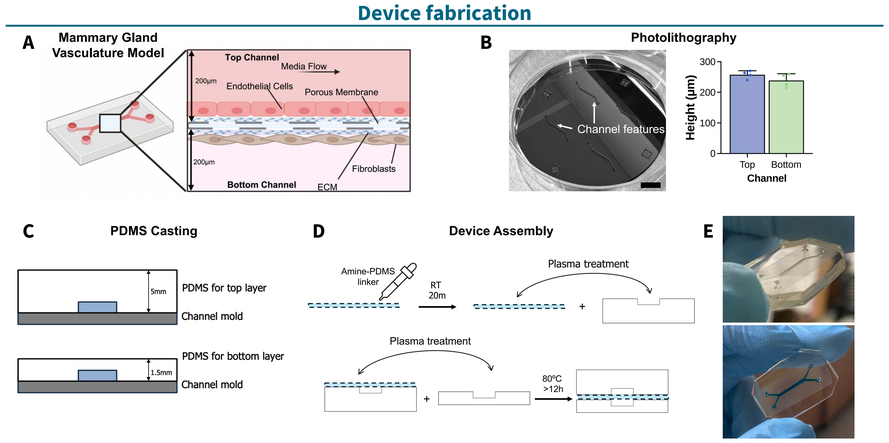

Figure 9: Microfluidic model fabrication. A. Schematic of cells cultured in microfluidic device. **B.** Image of SU8 channel mold and corresponding profilometry data. Scale bar is 10mm. Error bars are SD. **C.** PDMS casting to generate top and bottom layers of device. **D.** Procedure for assembling device. **E.** Images of final device.

Model validation and cell culture

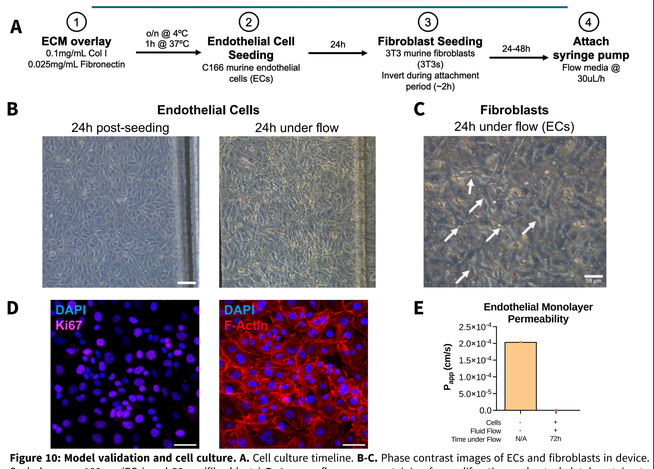

Figure 10: Model validation and cell culture. A. Cell culture timeline. **B-C.** Phase contrast images of ECs and fibroblasts in device. Scale bars are 100µm (ECs) and 50µm (fibroblasts) **D.** Immunofluorescence staining for proliferation and cytoskeletal proteins to confirm cell health. **E.** Quantification of top channel permeability via FITC-dextran permeability assay. n=1 independent experiment.

Conclusions and Ongoing Work

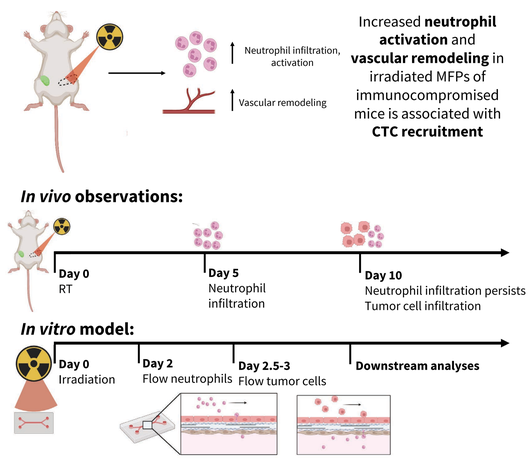

Acknowledgements

ViNSE
Focused Ultrasound Foundation
American Cancer Society
NIH National Cancer Institute